



# In situ grown heterojunction of Bi<sub>2</sub>WO<sub>6</sub>/BiOCl for efficient photoelectrocatalytic CO<sub>2</sub> reduction

Jixian Wang<sup>a</sup>, Yan Wei<sup>a</sup>, Bingjie Yang<sup>a</sup>, Bing Wang<sup>a</sup>, Jiazang Chen<sup>b</sup>, Huanwang Jing<sup>a,b,\*</sup>

<sup>a</sup> State Key Laboratory of Applied Organic Chemistry, College of Chemistry and Chemical Engineering, Lanzhou University, Lanzhou 730000, Gansu, China

<sup>b</sup> State Key Laboratory of Coal Conversion, Institute of Coal Chemistry, Chinese Academy of Sciences, Taiyuan 030001, Shanxi, China



## ARTICLE INFO

### Article history:

Received 23 April 2019

Revised 3 June 2019

Accepted 4 June 2019

### Keywords:

CO<sub>2</sub> reduction

Heterojunction

Photoelectrocatalysis

Charge separation efficiency

## ABSTRACT

CO<sub>2</sub> reduction is a very attractive research field in environmental, material, and chemical science in light of the energy crisis and the greenhouse effect. In this study, Bi<sub>2</sub>WO<sub>6</sub>/BiOCl heterojunctions were fabricated onto the F-SnO<sub>2</sub> transparent conductive glass in situ by a hydrothermal method. These new photocathodes, named BCW-X, were characterized by such methods as scanning electron microscopy, transmission electron microscopy, X-ray diffraction, X-ray photoelectron spectroscopy, and UV-vis spectra. Their morphology is a good 2D layered/3D flower structure. The exposed crystal plane of BiOCl was changed from (1 0 1) of the pristine form to (1 1 2) in the heterojunction. The photoelectrocatalytic reduction of CO<sub>2</sub> was carried out in BCW-X|KHCO<sub>3</sub>|BiVO<sub>4</sub> under irradiation by an Xe lamp and external voltage from a Si solar cell (−0.6 to −1.1 V). A PEC cell of BCW-6|KHCO<sub>3</sub>|BiVO<sub>4</sub> produces ethanol at a rate of 11.4 μM h<sup>−1</sup> cm<sup>−2</sup> (600 μmol h<sup>−1</sup> g<sup>−1</sup>) with 80.0% selectivity under −1.0 V. The apparent quantum efficiency is up to 0.63%, about three times that of composite BiOCl–Bi<sub>2</sub>WO<sub>6</sub> as photocathode. These phenomena can be attributed to the better photogenic electron–hole separation and high charge separation efficiency of heterojunctions.

© 2019 Elsevier Inc. All rights reserved.

## 1. Introduction

Along with fast development of human society, the total consumption of fossil fuels has been climbing to an unbelievable level, resulting in climate change and environment issues [1]. Therefore, it is of great significance to harvest and store solar energy [2] in chemical fuels by using abundant CO<sub>2</sub> and H<sub>2</sub>O via photocatalysis [3–5] and electrocatalysis [6–8]. Apart from the photocatalytic and electrocatalytic reduction of CO<sub>2</sub>, photoelectrocatalytic (PEC) CO<sub>2</sub> reduction [9–11] is also a promising method for the reduction of CO<sub>2</sub> into fuels and chemicals. PEC CO<sub>2</sub> reduction can integrate and optimize the advantages of photocatalysis and electrocatalysis to enhance their efficiency. The energetic photoelectrons could overcome the high overpotential of the electrochemical process and electrons from the circuit could prohibit the combination of photoelectrons and holes. To accelerate the sluggish kinetics of multielectron reactions, some co-catalysts, such as Au, Ag, Pt, Pd, Ru, Rh, Ir, and Re [12], were deposited on the surfaces of semiconductors.

Semiconductors such as TiO<sub>2</sub> [13], CdS [14], Ga<sub>2</sub>O<sub>3</sub> [15], ZnO [16], Si [17], and g-C<sub>3</sub>N<sub>4</sub> [18] have been used as catalysts in CO<sub>2</sub> reduction. Recently, much attention has been paid to Bi-based semiconductors in photocatalysis [19–23]. 2D layered semiconductors of bismuth oxyhalides (BiOX, X = Cl, Br, and I) have been applied to the degradation of hazardous pollutants [24], water splitting [25], and CO<sub>2</sub> conversion [26,27]. However, the wide band gaps of BiOX preclude their application under visible light [28]. Different strategies have been developed to overcome this drawback [29], including hierarchical nanostructures [30] and crystal-facet control [31]. On the other hand, various composites with heterostructures were constructed from BiOCl and other materials to augment their catalytic activity, such as graphene [32], metal oxides [33], metals [34,35], and salts [36].

As is well known, semiconductor heterojunctions can enhance the light absorption, the separation efficiency of electrons and holes, and the lifetime of photogenic carriers in hybrid materials [37]. The Zeng group has designed a TiO<sub>2</sub>/GaP *p–n* junction that enhances the separation efficiency of photogenic charges [38]. The Yu group has built a 2D/2D heterojunction of Ti<sub>3</sub>C<sub>2</sub>/Bi<sub>2</sub>WO<sub>6</sub> to improve photocatalytic CO<sub>2</sub> reduction [39]. Our group has reported Ti<sub>3</sub>C<sub>2</sub>/TiO<sub>2</sub> [40], g-C<sub>3</sub>N<sub>4</sub>/Ti<sub>3</sub>C<sub>2</sub> [41], and TiO<sub>2</sub>/ZnO [42] heterojunctions, showing evident improvements in PEC CO<sub>2</sub> reduction in water.

\* Corresponding author at: State Key Laboratory of Applied Organic Chemistry, College of Chemistry and Chemical Engineering, Lanzhou University, Lanzhou 730000, Gansu, China.

E-mail address: [hwjing@lzu.edu.cn](mailto:hwjing@lzu.edu.cn) (H. Jing).

Here, a new heterojunction of  $\text{Bi}_2\text{WO}_6/\text{BiOCl}$  was grown in situ onto an F-SnO<sub>2</sub> transparent conductive glass (FTO) surface and employed as a photocathode in the photoelectrocatalytic reduction of CO<sub>2</sub>. This PEC cell was a two-electrode system of BCW-X|KHCO<sub>3</sub>|BiVO<sub>4</sub> and performed CO<sub>2</sub> reduction under simulated sunlight irradiation and a tiny external voltage supplied by a Si solar cell.

## 2. Experimental

### 2.1. Preparation of the photocathode

#### 2.1.1. Preparation of BiOCl@FTO film electrodes

BiOCl electrodes were prepared according to the literature [43].  $\text{Bi}(\text{NO}_3)_3 \cdot 5\text{H}_2\text{O}$  (0.4815 g) and Triton X-100 (0.5 ml) were dissolved in 20 ml ethylene glycol to form a solution A. NaCl (0.117 g) was dissolved in 15 ml methanol to generate a solution B. Then the solutions A and B were mixed together and stirred for 2 h to get a clear solution C. FTO substrates (Nippon Sheet Glass) were ultrasonically cleaned in acetone, ethanol, and distilled water for 30 min each and immersed in a solution C in a 100-ml Teflon-lined stainless steel autoclave with the conductive side facing up. Then it was closed and solvothermal synthesis was conducted at 160 °C for 10 h. After the completion of the reaction, the FTO substrate was taken out, rinsed extensively with ultrapure water, and allowed to dry in ambient air.

#### 2.1.2. Preparation of Bi<sub>2</sub>WO<sub>6</sub>/BiOCl electrodes

The Bi<sub>2</sub>WO<sub>6</sub>/BiOCl heterojunction plates were prepared in situ by a hydrothermal method and weighed 2.0 mg for each plate. The as-prepared BiOCl precursors were immersed in 1 mmol Na<sub>2</sub>WO<sub>4</sub> aqueous solution in a 100-ml Teflon-lined stainless steel autoclave. The hydrothermal synthesis took place at 180 °C for 4, 6, 8, and 10 h for BCW-4, BCW-6, BCW-8, and BCW-10, respectively. After completion of the reaction, the electrodes were taken out of the autoclave, rinsed with ultrapure water, and calcined for 2 h at 500 °C in a muffle furnace.

### 2.2. Characterization of morphology and structure

A Hitachi S-4800 scanning electron microscope (SEM) was used to observe the morphology of samples. Transmission electron microscopy (TEM) and high-resolution transmission electron microscopy (HRTEM) of samples were performed on an FEI-Talos-F200s electron microscope. Their X-ray diffraction (XRD) patterns were collected on an X'Pert PRO diffractometer using

Cu K $\alpha$  radiation. The solid-state UV–vis absorption spectra of samples were collected on a UV–vis spectrophotometer (UV-2600, Shimadzu). The X-ray photoelectron spectroscopy (XPS) of BiOCl and BCW-4 was recorded on an XPS instrument (ESCALAB 210, VG Scientific) with an Mg K $\alpha$  X-ray resource. The spectra of various elements were calibrated according to C1s = 284.6 eV.

### 2.3. Photoelectrochemical measurement

The linear sweep voltammetry (LSV) curves of the photoelectrocatalytic cell were measured in a traditional three-electrode system on an electrochemical workstation (CHI660E). The prepared electrode served as a working electrode, BiVO<sub>4</sub> was employed as a counter electrode, and a saturated calomel electrode (SCE) was used as a reference electrode. The LSV experiments were conducted at a scan rate of 50 mV/s. The electrochemical impedance spectra (EIS) and the Mott–Schottky plots were both illustrated by the electrochemical workstation under EC conditions. On the other hand, the transient photocurrent responses were detected at –0.6 V with a two-electrode system.

### 2.4. Experiments on photocatalytic CO<sub>2</sub> reduction

PEC CO<sub>2</sub> reduction experiments were carried out in a closed quartz reactor of our own design equipped with a BiOCl or BCW-X photocathode and a BiVO<sub>4</sub> photoanode and powered by an external Si solar cell (–0.6 to –1.1 V). The electrolyte was an aqueous solution of KHCO<sub>3</sub> (0.1 M, 60 ml) containing Eosin Y as a photosensitizer (1 mM). The reactor was bubbled by CO<sub>2</sub> (99.998%) for 30 min and then irradiated by a 300-W Xenon lamp (Perfect Light Co.) for 2 h. After completion of experiments, the <sup>1</sup>H NMR spectra of liquid products were acquired by a NMR instrument (JNM-ECS400, JOEL) using dimethyl sulfoxide (DMSO, 10 mM) and m-trihydroxybenzene (MTB, 50 mM) as internal standards and the water suppression technique. Gas chromatography was employed to detect gas-phase products with a CP-3380 Varian instrument, calibrated with standard curves.

## 3. Results and discussion

### 3.1. Characterization of photocathodes

XRD patterns of BiOCl and BCW-4 are displayed in Fig. 1a. There are four characteristic peaks around 11.9°, 25.9°, 32.2°, and 33.5° that are attributed to diffraction of the crystal planes (0 0 1),

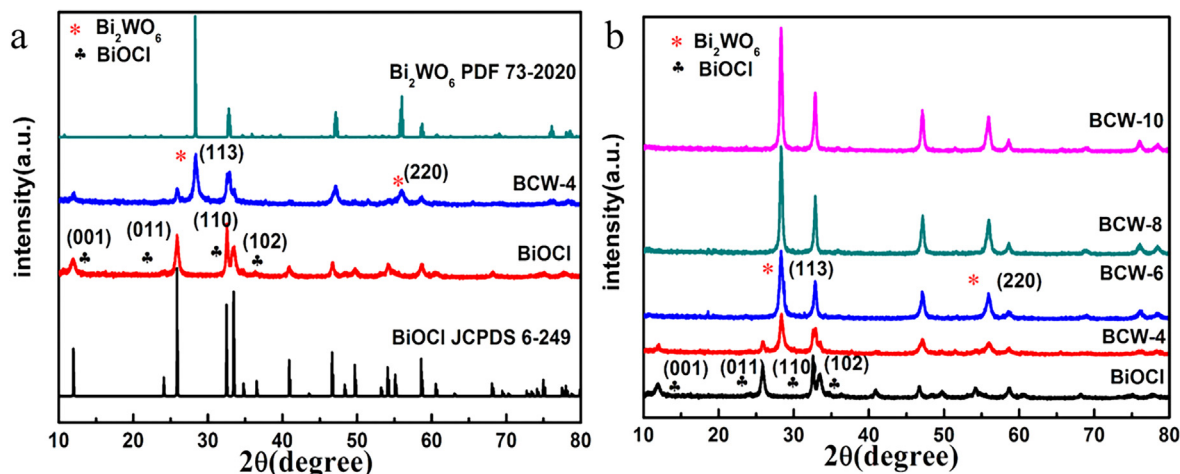


Fig. 1. XRD patterns of (a) BiOCl and BCW-4 and (b) BCW-X samples.

(0 1 1), (1 1 0), and (1 0 2) of tetragonal BiOCl, respectively. This is in good concordance with JCPDS card No. 6-249 [43]. The pattern of the BCW-4 heterojunction shows clearly two phases of BiOCl and Bi<sub>2</sub>WO<sub>6</sub> in which the peaks at 28.3° and 55.8° can be assigned to the diffraction of the (1 1 3) and (2 2 0) planes of Bi<sub>2</sub>WO<sub>6</sub>. When in situ growth time for the heterojunction is prolonged, the diffraction lines of BiOCl decrease, accompanied by an increase of diffraction lines for Bi<sub>2</sub>WO<sub>6</sub> (Fig. 1b).

The SEM images of BiOCl (Fig. 2a) show obviously good flower-like microspheres aggregated as nanosheets [43]. The thickness of BiOCl grown onto the FTO is about 7.5 μm (see Fig. S1a in the Supporting Information). When the Bi<sub>2</sub>WO<sub>6</sub> phase germinates

in situ from the matrix of BiOCl, the morphology of BCW-6 (Fig. 2b) still keeps the layered structure and the thickness of the heterojunction increases to 15 μm (Figs. S1b, S2).

The HRTEM (Fig. 2c) image of pure BiOCl illustrates multiple directions of the crystal plane (1 0 1) with  $d_{101} = 0.341$  nm. When the heterojunction of BCW-6 was formed, the crystal plane (1 1 3) of Bi<sub>2</sub>WO<sub>6</sub> and crystal plane (1 1 2) of BiOCl are obviously seen from the image of HRTEM (Fig. 2d). We can see that the exposed phase of BiOCl was changed from (1 0 1) to (1 1 2) due to good compatibility between the crystal planes (1 1 2) of BiOCl and (1 1 3) of Bi<sub>2</sub>WO<sub>6</sub>. To further prove the formation and structure of heterojunctions, their EDS mappings were obtained and

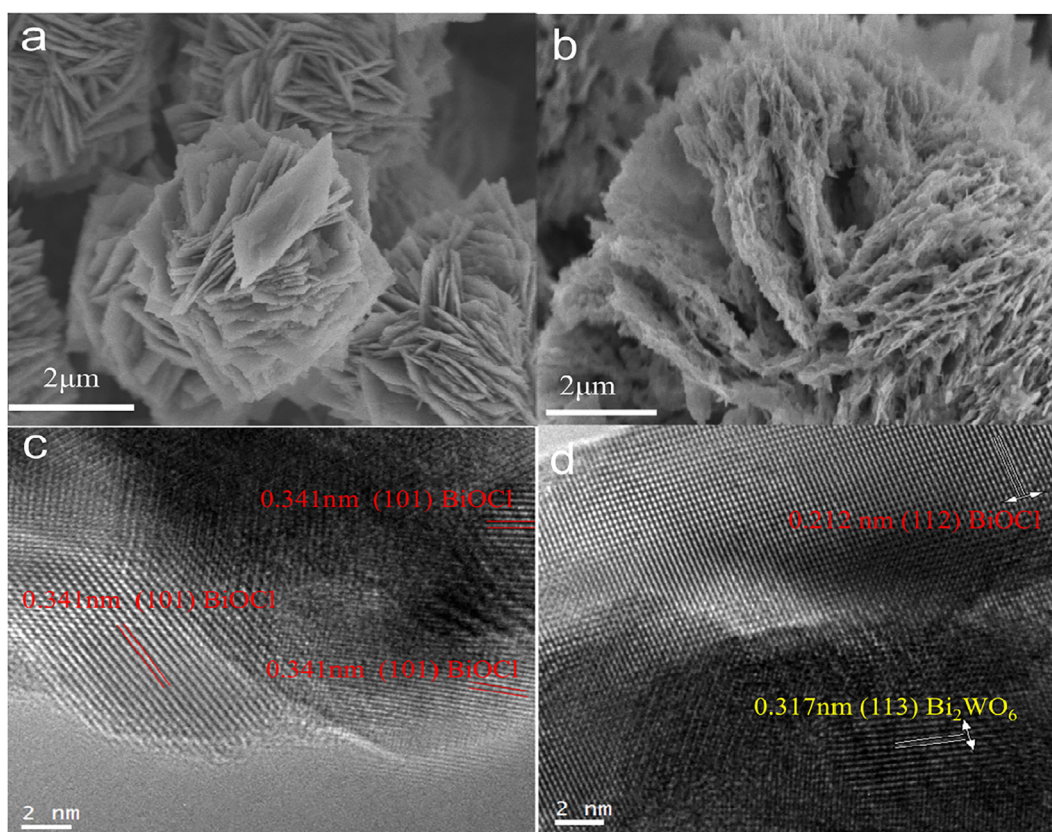


Fig. 2. SEM images of the photocathode, (a) BiOCl and (b) BCW-6, and HRTEM images of the photocathode, (c) BiOCl and (d) BCW-6.

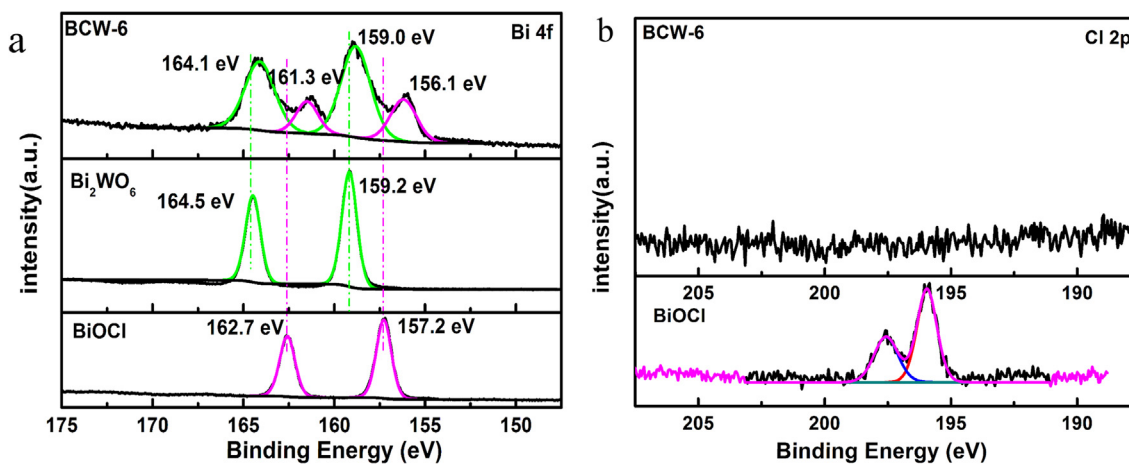


Fig. 3. Fine XPS spectra of (a) Bi 4f of BiOCl, Bi<sub>2</sub>WO<sub>6</sub> and BCW-6 and (b) Cl 2p of BiOCl and BCW-6.

revealed that W, Bi, Cl, and O are well distributed on the surface of the electrode BCW-6 (Fig. S3) in comparison with Bi, Cl, and O on BiOCl (Fig. S4).

The full XPS of heterojunction BCW-6 was investigated and depicted in Fig. S5. The fine XPS of Bi4f for BCW-6 has four peaks (Fig. 3a) that were assigned to the  $\text{Bi}_2\text{WO}_6$  phase (164.1 eV  $4f_{5/2}$  and 159.0 eV  $4f_{7/2}$ ) [44] and the BiOCl phase (161.3 eV  $4f_{5/2}$  and 156.1 eV  $4f_{7/2}$ ) in the heterojunction. Compared with the Bi4f orbitals in pure  $\text{Bi}_2\text{WO}_6$  (164.5 eV  $4f_{5/2}$  and 159.2 eV  $4f_{7/2}$ ) and BiOCl

(162.7 eV  $4f_{5/2}$  and 157.2 eV  $4f_{7/2}$ ), they have obvious red shifts. On the other hand, the peaks 195.9 eV ( $\text{Cl}2p_{3/2}$ ) and 197.5 eV ( $\text{Cl}2p_{1/2}$ ) appearing in BiOCl [45] could not be observed in heterojunctions due to the lower concentration of Cl in heterojunction BCW-6 (Fig. 3b). The concentrations of Bi, W, O, and Cl elements in heterojunction BCW-6 from EDX are shown in Table S1.

Solid UV–vis absorption spectra of photocathodes are shown in Fig. 4a. The spectra of the BiOCl electrode appear in the range 300–385 nm. When the heterojunction forms in the samples of BCW-X,

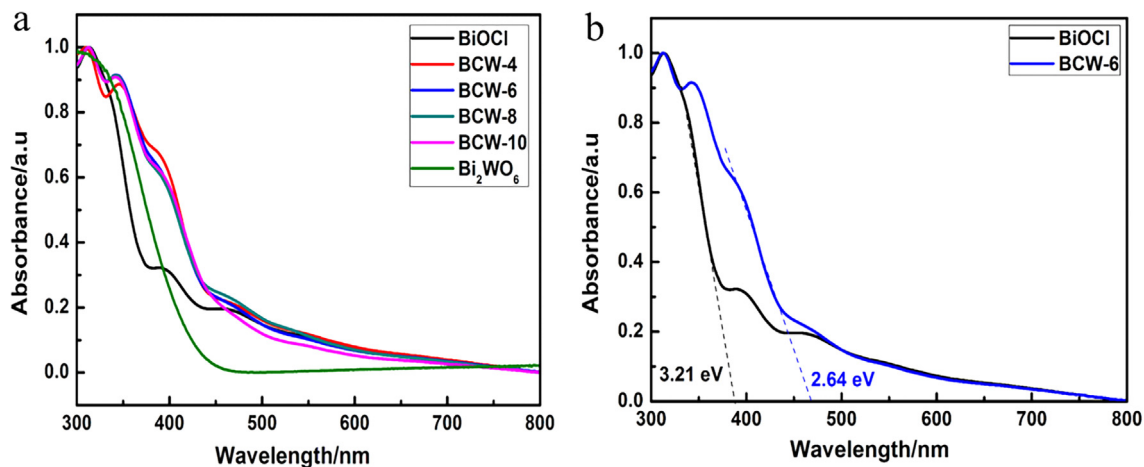


Fig. 4. (a) Normalized solid-state UV–vis absorption spectra of pure BiOCl and heterojunction electrodes. (b) The band gaps of BCW-6 and BiOCl electrodes.

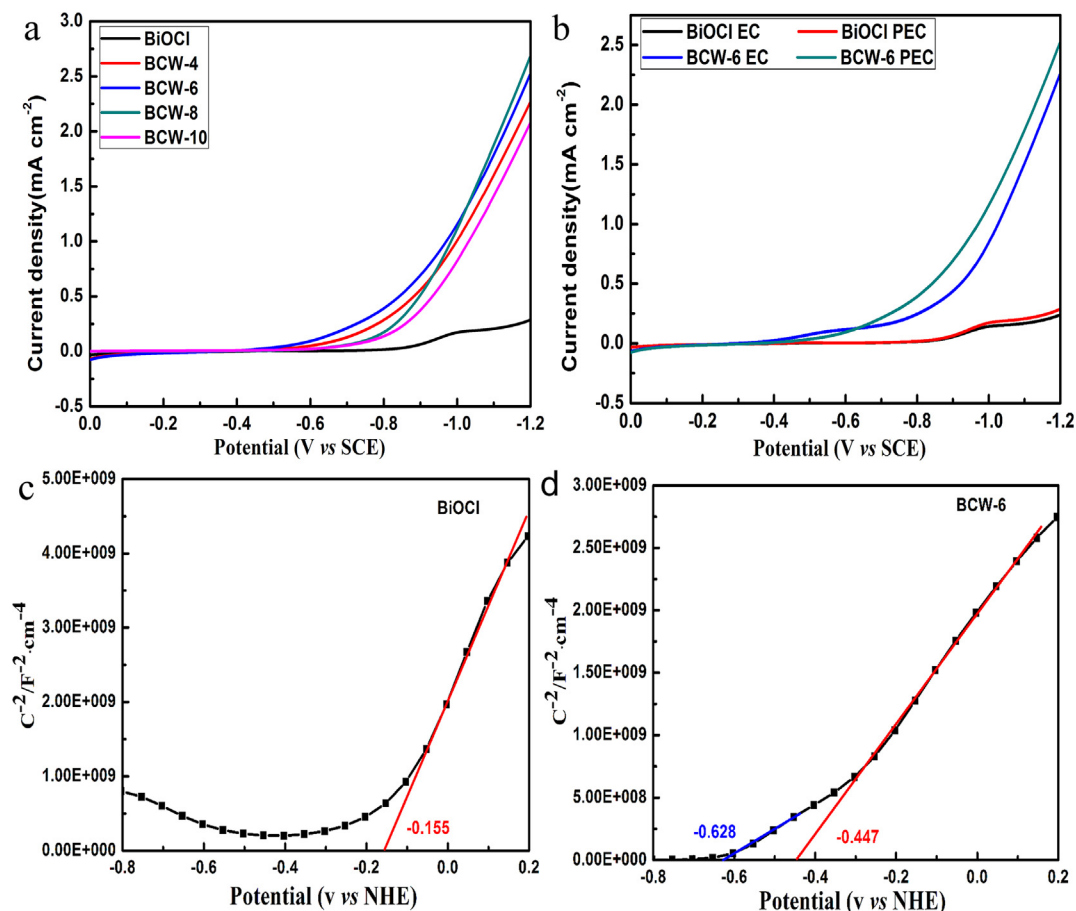


Fig. 5. (a) Photocurrent densities of PEC cells. (b) LSV curves of BiOCl and BCW-6 electrodes under EC and PEC conditions. Mott–Schottky plot of electrodes: (c) BiOCl, (d) BCW-6.

the absorption bands enlarge to 470 nm, which is superior to both BiOCl (385 nm) and Bi<sub>2</sub>WO<sub>6</sub> (425 nm) due to the interface of heterojunction. Therefore, the band gaps of heterojunctions BCW-X are narrowed. The band gap of BCW-6 is 2.64 eV (Fig. 4b). Other data of samples are presented in Fig. S6.

### 3.2. Photoelectrochemical properties of photocathodes

To understand the photoelectrocatalytic properties of photocathodes, their linear sweep voltammetry (LSV) curves were determined by a CHI660E electrochemical workstation with a three-electrode system under both EC and PEC conditions in the range of bias potential from 0 to -1.2 V (Fig. 5a, b). The photocurrent densities of BCW-X heterojunctions increase obviously with increasing bias potential from -0.6 V, compared with an almost a straight line near zero of BiOCl (Fig. 5a). This can be attributed to the contribution of heterojunction structure. On the other hand, the PEC current densities of heterojunctions are higher than their EC current densities owing to the contribution of photoelectrons (Figs. 5b, S7a).

To better understand the properties of semiconductors, their Mott-Schottky plots were measured and are shown in Figs. 5c, d, and S7. A positive slope for the BiOCl electrode suggests an *n*-type semiconductor (Fig. 5c). We can see from Figs. 5d and S7 that all heterojunctions of BCW-X have two positive slopes, indicating that these new heterojunctions are *n*-*n* homo-type heterojunctions [40]. Since the flat band potential of *n*-type semiconductor is close to the bottom edge of the conduction band, the intercepts collected in MS plots can be generally considered as conduction band (CB)

potentials [46]. Compared with a lower CB potential (vs. NHE) of pure BiOCl (-0.155 V), two CB potentials of photocathode BCW-6 appear at -0.628 V (Bi<sub>2</sub>WO<sub>6</sub>) and -0.447 V (BiOCl) that ensure appropriate redox potentials to produce ethanol and methanol [42].

The transient photocurrent curves of the photocathode were recorded at a constant bias of -0.6 V under chopped light irradiation and are depicted in Figs. S8a and 6a. Their photocurrent densities of BCW-X are higher than that of the precursor BiOCl due to the formation of heterojunctions. Generally, the spike formation of transient photocurrent is attributed to electron-hole recombination [47]. We can clearly see from Fig. 6a that there are no transient spikes in the transient photocurrent curves of heterojunction BCW-6. This phenomenon is ascribed to the high charge separation efficiency in heterojunctions.

To further understand the working mechanism of new heterojunctions in photoelectrocatalytic CO<sub>2</sub> reduction, the efficiency of charge separation ( $\eta_{\text{sep}}$ ) and charge transfer ( $\eta_{\text{trans}}$ ) were determined and calculated based on the current density of the PEC cell in the presence of Na<sub>2</sub>SO<sub>3</sub> ( $J_{\text{Na}_2\text{SO}_3}$ ) [48]. The data were calculated according to the equations

$$\eta_{\text{sep}} = J_{\text{Na}_2\text{SO}_3} / J_{\text{abs}}, \quad (1)$$

$$\eta_{\text{trans}} = J_{\text{KHCO}_3} / J_{\text{Na}_2\text{SO}_3}. \quad (2)$$

The  $J_{\text{abs}}$  can be calculated from a standard AM1.5G solar spectrum and experimental UV-vis spectra (Figs. 6b, c, S8). The detailed calculations can be found in the Supporting Information. The  $\eta_{\text{sep}}$  can be estimated by dividing the photocurrent density  $J_{\text{Na}_2\text{SO}_3}$

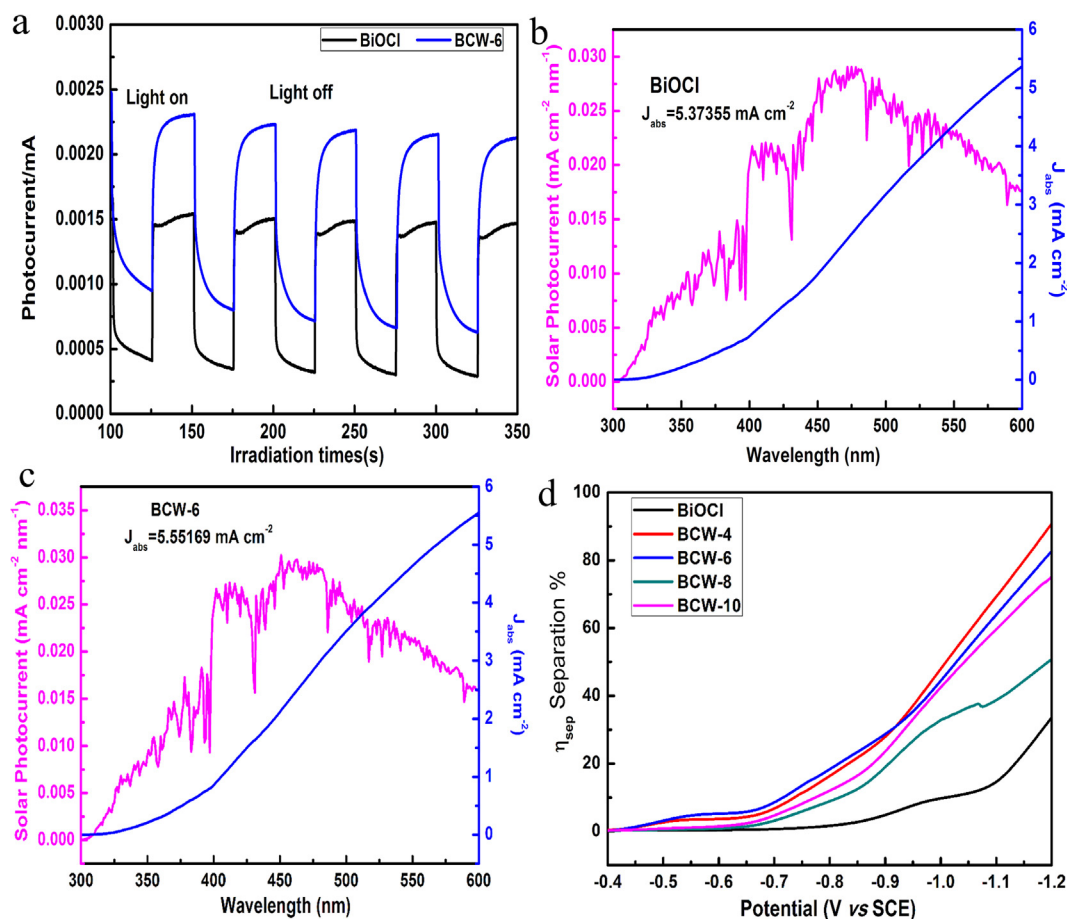


**Fig. 6.** (a) The transient photocurrent curves of BiOCl and BCW-6 electrodes. (b) The  $J_{\text{abs}}$  spectra of BiOCl and (c) BCW-6 electrodes. (d) The charge separation efficiency of BiOCl and BCW-X photocathodes.

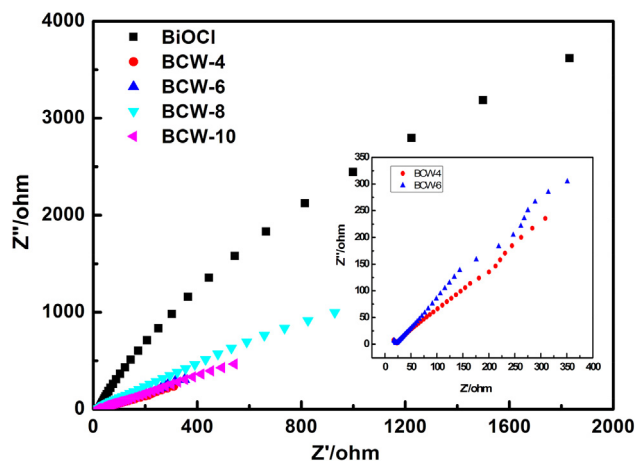


Fig. 7. Nyquist plots of different photocathodes.

(Fig. S9a) by  $J_{abs}$ , and are presented in Fig. 6d. It can be seen that the  $\eta_{sep}$  of all heterojunction electrodes are 3–5 times higher than the  $\eta_{sep}$  of BiOCl at  $-1.0$  V. The  $\eta_{trans}$  of working electrodes can be calculated with Eq. (2) using the data at bias potential  $-0.6$  V, the  $\eta_{trans}$  (Fig. S9b) of heterojunctions BCW-4, BCW-6, BCW-8, and BCW-10 are 24.9, 32.2, 31.2, and 30.1%, respectively, which are higher than 21.6% for BiOCl. This indicates that the mobility of carriers in heterojunctions is superior to that for the precursor BiOCl semiconductor.

To investigate the interfacial charge transfer between these photocathodes and the electrolyte, electrochemical impedance spectroscopy (EIS) was performed at  $-0.6$  V under dark conditions (Fig. 7). The  $R_{ct}$  values of heterojunctions are much lower than BiOCl, indicating higher mobility of electrons. Smaller cycles of BCW-4 and BCW-6 imply weak resistance that is beneficial for charge transfer [40].

### 3.3. Photoelectrocatalytic reduction of $CO_2$

Initially, the experiment was carried out by using BiOCl as a photocathode in the PEC cell BiOCl|KHCO<sub>3</sub>|BiVO<sub>4</sub> under  $-0.6$  V of external voltage (Fig. 8a), generating only a small amount of methanol (MeOH). When the heterojunction BCW-X was used as a photocathode, the PEC CO<sub>2</sub> reduction was investigated under external voltages of  $-0.6$ ,  $-0.8$ ,  $-1.0$ , and  $-1.1$  V. The PEC cell BCW-10|KHCO<sub>3</sub>|BiVO<sub>4</sub> yields methanol at a rate of  $12.5 \mu M h^{-1} cm^{-2}$  under  $-0.6$  V (Fig. 8a). The PEC cell BCW-10|KHCO<sub>3</sub>|BiVO<sub>4</sub> demonstrates an apparent quantum efficiency (AQE,  $\eta = 0.49\%$ ) that is 12 times higher than that of the PEC cell BiOCl|KHCO<sub>3</sub>|BiVO<sub>4</sub> ( $\eta = 0.04\%$ , Fig. 8c). Furthermore, the PEC cell BCW-6|KHCO<sub>3</sub>|BiVO<sub>4</sub> yields ethanol at a rate of  $11.4 \mu M h^{-1} cm^{-2}$  ( $600 \mu mol h^{-1} g^{-1}$ ) with 80.0% selectivity under  $-1.0$  V (Fig. 8b) that can be attributed to the morphology control [49]. It exhibits the highest AQE [50] (0.63%) under external voltage  $-1.0$  V in the PEC cell BCW-6|KHCO<sub>3</sub>|BiVO<sub>4</sub> (Fig. 8c). The <sup>1</sup>H NMR spectra of liquid products are displayed in Figs. S11–S14. In our new artificial photosynthesis system, O<sub>2</sub> was produced as well (Fig. S15).

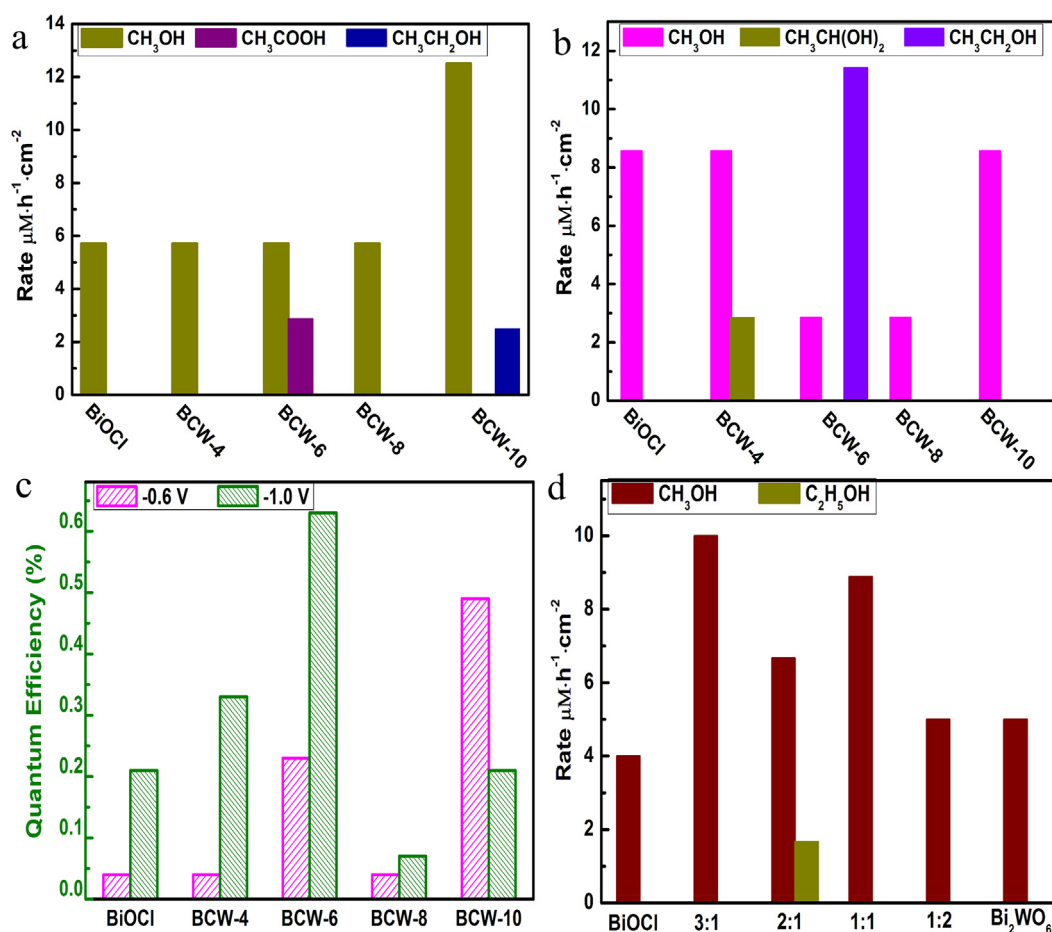


Fig. 8. The production rates of heterojunction PEC cells for five different photocathodes at (a)  $-0.6$  V and (b)  $-1.0$  V. (c) The apparent quantum efficiency of heterojunction PEC cells at  $-0.6$  and  $-1.0$  V. (d) The production rates of composite PEC cells at external voltage  $-1.0$  V.

**Table 1**  
Physical properties of heterojunction BCW-6 compared with those of the reported heterojunctions.

Material	Bi4f (XPS, eV)	Absorption bands (Uv-vis, nm)	Flat band (Mott-Schottky, V)	EIS ( $\Omega$ )	Ref.
Bi <sub>2</sub> WO <sub>6</sub> :BiOCl = 3:1	–	–	–	30,000	[52]
Bi <sub>2</sub> WO <sub>6</sub> /BiOCl	164.5, 159.2	431	–	–	[53]
BWO-PMS	164.6, 159.3	440	–0.42	–	[54]
BiOCl-Bi <sub>2</sub> WO <sub>6</sub>	163.8, 158.5	459	–	17,500	[51]
BiOCl-Bi <sub>2</sub> WO <sub>6</sub> (2:1) composite	164.6, 159.3	425	–0.285	713	This work
BCW-6 heterojunction	164.1, 159.0 161.3, 156.1	470	–0.447, –0.628	350	This work

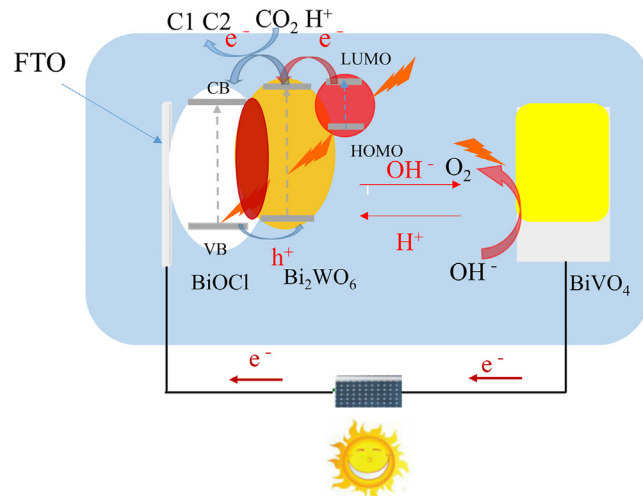
**Table 2**  
Performance of BCW-6 compared with the literatures of Bi-based materials.

Material	Condition	Main product	Rate ( $\mu\text{mol/g h}$ )	Ref.
BOC-OV	Photo	CO	16.76	[26]
HSA-Bi	Electro	HCOOH	–	[27]
Bi <sub>2</sub> WO <sub>6</sub> -HNRS	Photo	CH <sub>4</sub>	2.6	[55]
QDh-Bi <sub>2</sub> WO <sub>6</sub>	Photo	CH <sub>3</sub> OH	8.2	[56]
PtO <sub>x</sub> /Bi <sub>2</sub> WO <sub>6</sub>	Photo	CH <sub>4</sub>	108.8	[57]
TB2	Photo	CH <sub>3</sub> OH	0.44	[39]
BCW-6	Photoelectro	CH <sub>4</sub>	1.78	This work
		CH <sub>3</sub> CH <sub>2</sub> OH	600	
		CH <sub>3</sub> OH	151	

For comparison, four composite material samples were prepared by hydrothermal methods as well. The detailed procedure is described in the Supporting Information. The SEM images of reference samples exhibit blocky morphology (Figs. S16a–c). The HRTEM of composite material with a ratio of 3:1 for KCl/Na<sub>2</sub>WO<sub>4</sub> (Fig. S16d) demonstrates that the interfaces between the BiOCl and Bi<sub>2</sub>WO<sub>6</sub> phases are not compact. Solid UV–vis absorption spectra of photocathodes are shown in Fig. S17. The composite materials have absorption similar to that of pure Bi<sub>2</sub>WO<sub>6</sub>, which is better than in the previous report [51]. The LSV curves show that the composite materials with a ratio of 3:1 and 2:1 for KCl/Na<sub>2</sub>WO<sub>4</sub> have higher photocurrents than BiOCl and the composite materials with a ratio of 1:1 and 1:2 for KCl/Na<sub>2</sub>WO<sub>4</sub> have lower photocurrents than BiOCl at bias potentials from –0.9 to –1.2 V (Fig. S18a). Their Mott–Schottky plots suggest that BiOCl and Bi<sub>2</sub>WO<sub>6</sub> are n-type semiconductors (Fig. S18b, d). The conduction band position of the composite material (Fig. S18c) is between BiOCl and Bi<sub>2</sub>WO<sub>6</sub>, like a simple mixture and different from a heterojunction. The formation rates of liquid products are depicted in Fig. 8d and show that methanol was the major product in the composite material. When composite BiOCl–Bi<sub>2</sub>WO<sub>6</sub> was used as a photocathode, its apparent quantum efficiency was reduced to 0.24% due to higher  $R_{\text{ct}}$  (Fig. S19) leading to lower mobility of electrons.

### 3.4. Comparison with the literature

For better understanding of the advantages of new Bi<sub>2</sub>WO<sub>6</sub>/BiOCl heterojunctions, the physical properties of BCW-6 are compared with the literature (Table 1). We can see that they demonstrate excellent absorption of solar light, small  $R_{\text{ct}}$ , and four XPS peaks of Bi4f that clearly differ from those for the reported heterojunctions. To the best of our knowledge, this is the first attempt to apply the Bi<sub>2</sub>WO<sub>6</sub>/BiOCl heterojunction in CO<sub>2</sub> reduction. The BCW-6 heterojunction yields ethanol at a rate of 600  $\mu\text{mol h}^{-1} \text{g}^{-1}$  and methanol at a rate of 151  $\mu\text{mol h}^{-1} \text{g}^{-1}$ . The total rate of carbon-based products is 12.4–606.8 times higher than in the literature (Table 2). This result is really superior to the reported results, due to the excellent properties of new heterojunctions.



**Scheme 1.** A proposed mechanism for the PEC cell with Bi<sub>2</sub>WO<sub>6</sub>/BiOCl heterojunction.

### 3.5. Proposed mechanism of photoelectrocatalytic system

According to our experimental results for the PEC cell, a possible mechanism for PEC CO<sub>2</sub> reduction to chemical fuels is proposed and illustrated in Scheme 1. The electrons in the ground state of Bi<sub>2</sub>WO<sub>6</sub> and the dye molecules could jump to the excited state under light irradiation. The generated photoelectrons transfer to the CB band of BiOCl through the heterojunction. Then the photoelectrons can combine with protons to generate active hydrogen atoms, which can immediately reduce CO<sub>2</sub> to hydrocarbon. Meanwhile, hydroxyl groups (OH<sup>–</sup>) transfer to the photoanode of BiVO<sub>4</sub> and are oxidized to O<sub>2</sub>.

## 4. Conclusions

In summary, in situ grown Bi<sub>2</sub>WO<sub>6</sub>/BiOCl heterojunctions were designed, prepared, and applied to PEC CO<sub>2</sub> reduction for the first time. These new heterojunctions of BCW-X electrodes in the PEC

cell BCW-X|K<sub>2</sub>CO<sub>3</sub>|BiVO<sub>4</sub> demonstrate an excellent ability to convert water and CO<sub>2</sub> molecules to hydrocarbons at a low external voltage under irradiation with simulated sunlight. The heterojunctions of BCW-X retain a good 2D layered structure with the lattice change from (1 0 1) to (1 1 2) for BiOCl, improving the efficiency of photoelectron–hole separation. The best heterojunction of BCW-6 exhibits the highest apparent quantum efficiency (0.63%), which is higher than 0.4% of natural plants.

## Acknowledgments

This study was funded by the Natural Science Foundation of Gansu Province (17JR5RA212) and the Foundation of State Key Laboratory of Coal Conversion (J19-20-913-1). We thank the Electron Microscopy Center of Lanzhou University for the microscopy and microanalysis of our specimens.

## Appendix A. Supplementary material

Supplementary data to this article can be found online at <https://doi.org/10.1016/j.jcat.2019.06.007>.

## References

- [1] C. Long, X. Li, J. Guo, Y. Shi, S. Liu, Z. Tang, Electrochemical reduction of CO<sub>2</sub> over heterogeneous catalysts in aqueous solution: recent progress and perspectives, *Small Methods* (2018) 1800369.
- [2] N.S. Lewis, Research opportunities to advance solar energy utilization, *Science* 351 (6271) (2016) 1920.
- [3] Y. Wang, N.Y. Huang, J.Q. Shen, P.Q. Liao, X.M. Chen, J.P. Zhang, Hydroxide ligands cooperate with catalytic centers in metal-organic frameworks for efficient photocatalytic CO<sub>2</sub> reduction, *J. Am. Chem. Soc.* 140 (1) (2018) 38–41.
- [4] Y. Wang, Z. Zhang, L. Zhang, Z. Luo, J. Shen, H. Lin, J. Long, J.C.S. Wu, X. Fu, X. Wang, C. Li, Visible-light driven overall conversion of CO<sub>2</sub> and H<sub>2</sub>O to CH<sub>4</sub> and O<sub>2</sub> on 3D-SiC@2D-MoS<sub>2</sub> heterostructure, *J. Am. Chem. Soc.* 140 (44) (2018) 14595–14598.
- [5] J. Low, L. Zhang, T. Tong, B. Shen, J. Yu, TiO<sub>2</sub>/MXene Ti<sub>3</sub>C<sub>2</sub> composite with excellent photocatalytic CO<sub>2</sub> reduction activity, *J. Catal.* 361 (2018) 255–266.
- [6] L.D. Chen, M. Urushihara, K. Chan, J.K. Nørskov, Electric field effects in electrochemical CO<sub>2</sub> reduction, *ACS Catal.* 6 (10) (2016) 7133–7139.
- [7] D.A. Vermaas, W.A. Smith, Synergistic electrochemical CO<sub>2</sub> reduction and water oxidation with a bipolar membrane, *ACS Energy Lett.* 1 (6) (2016) 1143–1148.
- [8] C. Cui, J. Han, X. Zhu, X. Liu, H. Wang, D. Mei, Q. Ge, Promotional effect of surface hydroxyls on electrochemical reduction of CO<sub>2</sub> over SnO/Sn electrode, *J. Catal.* 343 (2016) 257–265.
- [9] L. Wang, Y. Jia, R. Nie, Y. Zhang, F. Chen, Z. Zhu, J. Wang, H. Jing, Ni-foam-supported and amine-functionalized TiO<sub>2</sub> photocathode improved photoelectrocatalytic reduction of CO<sub>2</sub> to methanol, *J. Catal.* 349 (2017) 1–7.
- [10] S. Kaneko, H. Katsumata, T. Suzuki, K. Ohta, Photoelectrocatalytic reduction of CO<sub>2</sub> in LiOH/methanol at metal-modified p-InP electrodes, *Appl. Catal. B Environ.* 64 (1–2) (2006) 139–145.
- [11] J. Cheng, M. Zhang, G. Wu, X. Wang, J. Zhou, K. Cen, Photoelectrocatalytic reduction of CO<sub>2</sub> into chemicals using Pt-modified reduced graphene oxide combined with Pt-modified TiO<sub>2</sub> nanotubes, *Environ. Sci. Technol.* 48 (12) (2014) 7076–7084.
- [12] X. Chang, T. Wang, P. Yang, G. Zhang, J. Gong, The development of cocatalysts for photoelectrochemical CO<sub>2</sub> reduction, *Adv. Mater.* 1804710 (2018).
- [13] S.N. Habisreutinger, L. Schmidt-Mende, J.K. Stolarczyk, Photocatalytic reduction of CO<sub>2</sub> on TiO<sub>2</sub> and other semiconductors, *Angew. Chem. Int. Ed.* 52 (29) (2013) 7372–7408.
- [14] Y.S. Chaudhary, T.W. Woolerton, C.S. Allen, J.H. Warner, E. Pierce, S.W. Ragsdale, F.A. Armstrong, Visible light-driven CO<sub>2</sub> reduction by enzyme coupled CdS nanocrystals, *Chem. Commun.* 48 (1) (2012) 58–60.
- [15] M. Yamamoto, T. Yoshida, N. Yamamoto, T. Nomoto, Y. Yamamoto, S. Yagi, H. Yoshida, Photocatalytic reduction of CO<sub>2</sub> with water promoted by Ag clusters in Ag/Ga<sub>2</sub>O<sub>3</sub> photocatalysts, *J. Mater. Chem. A* 3 (32) (2015) 16810–16816.
- [16] C. Xin, M. Hu, K. Wang, X. Wang, Significant enhancement of photocatalytic reduction of CO<sub>2</sub> with H<sub>2</sub>O over ZnO by the formation of basic zinc carbonate, *Langmuir* 33 (27) (2017) 6667–6676.
- [17] C. Li, T. Wang, B. Liu, M. Chen, A. Li, G. Zhang, M. Du, H. Wang, S.F. Liu, J. Gong, Photoelectrochemical CO<sub>2</sub> reduction to adjustable syngas on grain-boundary-mediated a-Si/TiO<sub>2</sub>/Au photocathodes with low onset potentials, *Energy Environ. Sci.* (2019).
- [18] S. Cao, Y. Li, B. Zhu, M. Jaroniec, J. Yu, Facet effect of Pd cocatalyst on photocatalytic CO<sub>2</sub> reduction over g-C<sub>3</sub>N<sub>4</sub>, *J. Catal.* 349 (2017) 208–217.
- [19] J. Xiong, Q. Dong, T. Wang, Z. Jiao, G. Lu, Y. Bi, Direct conversion of Bi nanospheres into 3D flower-like BiOBr nanoarchitectures with enhanced photocatalytic properties, *RSC Adv.* 4 (2) (2014) 583–586.
- [20] J. Xiong, Z. Jiao, G. Lu, W. Ren, J. Ye, Y. Bi, Facile and rapid oxidation fabrication of BiOCl hierarchical nanostructures with enhanced photocatalytic properties, *Chemistry* 19 (29) (2013) 9472–9475.
- [21] M. Guan, C. Xiao, J. Zhang, S. Fan, R. An, Q. Cheng, J. Xie, M. Zhou, B. Ye, Y. Xie, Vacancy associates promoting solar-driven photocatalytic activity of ultrathin bismuth oxychloride nanosheets, *J. Am. Chem. Soc.* 135 (28) (2013) 10411–10417.
- [22] D. Mao, J. Yuan, X. Qu, C. Sun, S. Yang, H. He, Size tunable Bi<sub>3</sub>O<sub>4</sub>Br hierarchical hollow spheres assembled with {0 0 1}-facets exposed nanosheets for robust photocatalysis against phenolic pollutants, *J. Catal.* 369 (2019) 209–221.
- [23] S.Y. Chai, Y.J. Kim, M.H. Jung, A.K. Chakraborty, D. Jung, W.I. Lee, Heterojunctioned BiOCl/Bi<sub>2</sub>O<sub>3</sub>, a new visible light photocatalyst, *J. Catal.* 262 (1) (2009) 144–149.
- [24] Y. Ao, J. Bao, P. Wang, C. Wang, J. Hou, Bismuth oxychloride modified titanium phosphate nanoplates: a new p-n type heterostructured photocatalyst with high activity for the degradation of different kinds of organic pollutants, *J. Colloid Interface Sci.* 476 (2016) 71–78.
- [25] W. Fan, C. Li, H. Bai, Y. Zhao, B. Luo, Y. Li, Y. Ge, W. Shi, H. Li, An in situ photoelectroreduction approach to fabricate Bi/BiOCl heterostructure photocathodes: understanding the role of Bi metal for solar water splitting, *J. Mater. Chem. A* 5 (10) (2017) 4894–4903.
- [26] Z. Ma, P. Li, L. Ye, Y. Zhou, F. Su, C. Ding, H. Xie, Y. Bai, P.K. Wong, Oxygen vacancies induced exciton dissociation of flexible BiOCl nanosheets for effective photocatalytic CO<sub>2</sub> conversion, *J. Mater. Chem. A* 5 (47) (2017) 24995–25004.
- [27] H. Zhang, Y. Ma, F. Qian, J. Huang, F. Jia, L. Zhang, Selective electro-reduction of CO<sub>2</sub> to formate on nanostructured Bi from reduction of BiOCl nanosheets, *Electrochem. Commun.* 46 (2014) 63–66.
- [28] W.L. Huang, Q. Zhu, Electronic structures of relaxed BiOX (X=F, Cl, Br, I) photocatalysts, *Comput. Mater. Sci.* 43 (4) (2008) 1101–1108.
- [29] Y. Yu, C. Cao, H. Liu, P. Li, F. Wei, Y. Jia, W. Song, A Bi/BiOCl heterojunction photocatalyst with enhanced electron–hole separation and excellent visible light photodegrading activity, *J. Mater. Chem. A* 2 (6) (2014) 1677–1681.
- [30] H. Gnayem, Y. Sasson, Hierarchical nanostructured 3D flowerlike BiOClxBr 1–x semiconductors with exceptional visible light photocatalytic activity, *ACS Catal.* 3 (2) (2013) 186–191.
- [31] J. Jiang, K. Zhao, X. Xiao, L. Zhang, Synthesis and facet-dependent photoreactivity of BiOCl single-crystalline nanosheets, *J. Am. Chem. Soc.* 134 (10) (2012) 4473–4476.
- [32] F. Gao, D. Zeng, Q. Huang, S. Tian, C. Xie, Chemically bonded graphene/BiOCl nanocomposites as high-performance photocatalysts, *PhysChemChemPhys* 14 (30) (2012) 10572–10578.
- [33] S. Shamaila, A.K.L. Sajjad, F. Chen, J. Zhang, WO<sub>3</sub>/BiOCl, a novel heterojunction as visible light photocatalyst, *J. Colloid Interface Sci.* 356 (2) (2011) 465–472.
- [34] L. Ye, J. Liu, C. Gong, L. Tian, T. Peng, L. Zan, Two different roles of metallic Ag on Ag/AgX/BiOX (X = Cl, Br) visible light photocatalysts: surface plasmon resonance and Z-scheme bridge, *ACS Catal.* 2 (8) (2012) 1677–1683.
- [35] L. Zhang, W. Wang, S. Sun, Y. Sun, E. Gao, J. Xu, Water splitting from dye wastewater: a case study of BiOCl/copper(II) phthalocyanine composite photocatalyst, *Appl. Catal. B Environ.* 132–133 (2013) 315–320.
- [36] B. Cao, P. Dong, S. Cao, Y. Wang, T. Gur, BiOCl/Ag<sub>3</sub>PO<sub>4</sub> composites with highly enhanced ultraviolet and visible light photocatalytic performances, *J. Am. Ceram. Soc.* (2012) 544–548.
- [37] J. Li, N. Wu, Semiconductor-based photocatalysts and photoelectrochemical cells for solar fuel generation: a review, *Catal. Sci. Technol.* 5 (3) (2015) 1360–1384.
- [38] G. Zeng, J. Qiu, Z. Li, P. Pavaskar, S.B. Cronin, CO<sub>2</sub> reduction to methanol on TiO<sub>2</sub>-passivated GaP photocatalysts, *ACS Catal.* 4 (10) (2014) 3512–3516.
- [39] S. Cao, B. Shen, T. Tong, J. Fu, J. Yu, 2D/2D heterojunction of ultrathin MXene/Bi<sub>2</sub>WO<sub>6</sub> nanosheets for improved photocatalytic CO<sub>2</sub> reduction, *Adv. Funct. Mater.* 28 (21) (2018) 1800136.
- [40] Y. Xu, S. Wang, J. Yang, B. Han, R. Nie, J. Wang, H. Jing, In-situ grown nanocrystal TiO<sub>2</sub> on 2D Ti<sub>3</sub>C<sub>2</sub> nanosheets for artificial photosynthesis of chemical fuels, *Nano Energy* 51 (2018) 442–450.
- [41] Y. Xu, S. Wang, J. Yang, B. Han, R. Nie, J. Wang, Y. Dong, X. Yu, J. Wang, H. Jing, Highly efficient photoelectrocatalytic reduction of CO<sub>2</sub> on the Ti<sub>3</sub>C<sub>2</sub>/g-C<sub>3</sub>N<sub>4</sub> heterojunction with rich Ti<sup>3+</sup> and pyri-N species, *J. Mater. Chem. A* 6 (31) (2018) 15213–15220.
- [42] B. Han, J. Wang, C. Yan, Y. Dong, Y. Xu, R. Nie, H. Jing, The photoelectrocatalytic CO<sub>2</sub> reduction on TiO<sub>2</sub>@ZnO heterojunction by tuning the conduction band potential, *Electrochim. Acta* 285 (2018) 23–29.
- [43] Q. Mu, Q. Zhang, H. Wang, Y. Li, Facile growth of vertically aligned BiOCl nanosheet arrays on conductive glass substrate with high photocatalytic properties, *J. Mater. Chem.* 22 (33) (2012) 16851.
- [44] B.V. Kumar, M.D. Prasad, M. Vithal, Enhanced visible light photocatalytic activity of Sn doped Bi<sub>2</sub>WO<sub>6</sub> nanocrystals, *Mater. Lett.* 152 (2015) 200–202.
- [45] Y. Hou, J. Liu, Z. Li, Z. Wu, K. Zhu, Q. Xi, J. Zhuang, J. Chen, G. Qian, M. Cong, Construction of novel BiOCl/MoS<sub>2</sub> nanocomposites with Z-scheme structure for enhanced photocatalytic activity, *Mater. Lett.* 218 (2018) 110–114.
- [46] A. Jin, Y. Jia, C. Chen, X. Liu, J. Jiang, X. Chen, F. Zhang, Efficient photocatalytic hydrogen evolution on band structure tuned polytriazine/heptazine based carbon nitride heterojunctions with ordered needle-like morphology achieved by an in situ molten salt method, *J. Phys. Chem. C* 121 (39) (2017) 21497–21509.

- [47] F. Li, J. Li, J. Zhang, L. Gao, X. Long, Y. Hu, S. Li, J. Jin, J. Ma, NiO nanoparticles anchored on phosphorus-doped  $\alpha$ -Fe<sub>2</sub>O<sub>3</sub> nanoarrays: an efficient hole extraction p-n heterojunction photoanode for water oxidation, *ChemSusChem* 11 (13) (2018) 2156–2164.
- [48] Z. Zhang, Y. Li, X. Jiang, W. Han, M. Xie, F. Wang, E. Xie, Significantly improved charge collection and interface injection in 3D BiVO<sub>4</sub> based multilayered core-shell nanowire photocatalysts, *Nanoscale* 9 (37) (2017) 14015–14022.
- [49] J. Wang, B. Han, R. Nie, Y. Xu, X. Yu, Y. Dong, J. Wang, H. Jing, Photoelectrocatalytic reduction of CO<sub>2</sub> to chemicals via ZnO@nickel foam: controlling C-C coupling by ligand or morphology, *Top. Catal.* 61 (15–17) (2018) 1563–1573.
- [50] Y. Zhang, B. Han, Y. Xu, D. Zhao, Y. Jia, R. Nie, Z. Zhu, F. Chen, J. Wang, H. Jing, Artificial photosynthesis of alcohols by multi-functionalized semiconductor photocathodes, *ChemSusChem* 10 (8) (2017) 1742–1748.
- [51] W. Yang, B. Ma, W. Wang, Y. Wen, D. Zeng, B. Shan, Enhanced photosensitized activity of a BiOCl–Bi<sub>2</sub>WO<sub>6</sub> heterojunction by effective interfacial charge transfer, *PhysChemChemPhys* 15 (44) (2013) 19387.
- [52] Z. Liang, C. Zhou, J. Yang, Q. Mo, Y. Zhang, Y. Tang, Visible light responsive Bi<sub>2</sub>WO<sub>6</sub> /BiOCl heterojunction with enhanced photocatalytic activity for degradation of tetracycline and rhodamine B, *Inorg. Chem. Commun.* 93 (2018) 136–139.
- [53] S. Zhu, C. Yang, F. Li, T. Li, M. Zhang, W. Cao, Improved photocatalytic Bi<sub>2</sub>WO<sub>6</sub> / BiOCl heterojunctions: one-step synthesis via an ionic-liquid assisted ultrasonic method and first-principles calculations, *Mol. Catal.* 435 (2017) 33–48.
- [54] Q. Yang, M. Luo, K. Liu, H. Cao, H. Yan, A composite of single-crystalline Bi<sub>2</sub>WO<sub>6</sub> and polycrystalline BiOCl with a high percentage of exposed (001) facets for highly efficient photocatalytic degradation of organic pollutants, *Chem. Commun.* 55 (40) (2019) 5728–5731.
- [55] L. Xiao, R. Lin, J. Wang, C. Cui, J. Wang, Z. Li, A novel hollow-hierarchical structured Bi<sub>2</sub>WO<sub>6</sub> with enhanced photocatalytic activity for CO<sub>2</sub> photoreduction, *J. Colloid Interface Sci.* 523 (2018) 151–158.
- [56] Z. Jiang, X. Liang, H. Zheng, Y. Liu, Z. Wang, P. Wang, X. Zhang, X. Qin, Y. Dai, M.-H. Whangbo, B. Huang, Photocatalytic reduction of CO<sub>2</sub> to methanol by three-dimensional hollow structures of Bi<sub>2</sub>WO<sub>6</sub> quantum dots, *Appl. Catal. B Environ.* 219 (2017) 209–215.
- [57] Q. Wang, K. Wang, L. Zhang, H. Wang, W. Wang, Photocatalytic reduction of CO<sub>2</sub> to methane over PtOx-loaded ultrathin Bi<sub>2</sub>WO<sub>6</sub> nanosheets, *Appl. Surf. Sci.* 470 (2019) 832–839.